# Experimental-like Helical Self-Organization in Reversed-Field Pinch Modeling

D. Bonfiglio,[1,*] M. Veranda,[1] S. Cappello,[1] D. F. Escande,[2,1] and L. Chacón[3]
[1]Consorzio RFX, Associazione Euratom-ENEA sulla Fusione, 35127 Padova, Italy
[2]Aix-Marseille Université, CNRS, PIIM, UMR 7345, 13013 Marseille, France
[3]Los Alamos National Laboratory, Los Alamos, New Mexico 87545, USA
(Received 17 July 2013; published 21 August 2013)

We report the first nonlinear three-dimensional magnetohydrodynamic (MHD) numerical simulations of the reversed-field pinch (RFP) that exhibit a systematic repetition of quasisingle helicity states with the same dominant mode in between reconnection events. This distinctive feature of experimental self-organized helical RFP plasmas is reproduced in MHD simulations at low dissipation by allowing a helical modulation of the plasma magnetic boundary similar to the experimental one. Realistic mode amplitudes and magnetic topology are also found.

DOI: 10.1103/PhysRevLett.111.085002 PACS numbers: 52.65.Kj, 05.45.−a, 52.35.Py, 52.55.Hc

The reversed-field pinch (RFP) is a toroidal configuration for magnetic confinement of fusion plasmas [1,2]. As in the tokamak [3], a toroidal current is driven in the plasma contributing a poloidal component to the confining magnetic field. However, for a given plasma current, the toroidal magnetic field in the RFP is one order of magnitude smaller than in the tokamak. In addition, the toroidal field distribution is strongly determined by internal currents via the so-called RFP dynamo effect (see [1,2,4–6] and references therein). The RFP dynamo sustains the characteristic sign reversal at the plasma edge and only a small toroidal flux is produced by external coils. Such a small edge magnetic field and the potential of reaching ignition by Ohmic heating alone [7] would greatly simplify a fusion reactor design based on this configuration, eliminating or reducing the need of superconducting coils and additional heating systems. On the other hand, as yet, the level of confinement in the RFP is typically not as good as the tokamak one, due to the magnetohydrodynamic (MHD) activity which can develop in such a self-organized configuration, spoiling the order of the magnetic topology. In recent years, however, a promising way to improve the confinement of RFP plasmas has been extensively investigated. The approach exploits the tendency of RFP plasmas to self-organize into quasisingle helicity (QSH) states, as observed in all major RFP devices [8–11]. QSH plasmas are actively investigated in the two largest RFP experiments, the RFX-mod [12] and MST [13] devices. The QSH regime is characterized by one (dominant) nonlinearly saturated kink-tearing mode, of significantly larger amplitude than other (secondary) MHD modes. QSH plasmas are preferentially observed when increasing the plasma current [14,15]. At high current, long-lasting helical states develop [10,16], which share similarities with helical states in the tokamak (like the ''snake'' phenomenon [17] and the helical hybrid scenario proposed for ITER [18]) as well as with the stellarator concept [19–21]. Long-lived ordered large scale helical fields are also observed in astrophysical plasmas such as relativistic jets [22] or solar prominences related to emerging helical flux ropes [23]. Helical RFP states display better confinement properties than multiple helicity (MH) states, characterized by comparable amplitudes of the most active MHD modes. In particular, the occurrence of internal transport barriers is observed when the so-called single-helical axis (SHAx) state [10,24] is achieved. QSH phases are periodically interrupted by magnetic reconnection events [25] associated with enhanced dynamo modes activity and formation of current sheets [14,26,27].

Self-organized helical RFP states were observed in nonlinear three-dimensional (3D) viscoresistive MHD simulations with ideal boundary conditions (BCs) long before the experimental discovery of QSH plasmas [28–30]. Within this framework, the dynamical regime is ruled by the amount of viscoresistive dissipation, as measured by the Hartmann number $H \equiv (\eta\nu)^{-1/2}$, with $\eta$ and $\nu$ being dimensionless resistivity and viscosity parameters [31,32]. The bifurcation to stationary, pure single-helicity Ohmic equilibrium solutions occurs at high dissipation, below the threshold $H_c \simeq 2000$. At low dissipation, a sawtoothing MH regime with quasiperiodic reconnection events, similar to those occurring in the experiment, is found [32–37]. Intermittent QSH phases reminiscent of experimental ones are observed at intermediate dissipation [32]. However, the distinctive experimental feature of the systematic repetition of QSH phases with the same dominant mode in between reconnection events have never been reproduced by 3D MHD codes, either within the simple viscoresistive model [32,38,39] or when using more refined models of the magnetic boundary [40] or of the plasma itself [41,42]. Thus, a satisfactory agreement with respect to experimental observations has been lacking so far. The study described in this Letter is motivated by this fact, which pertains to the general critical problem of the validation of advanced numerical modeling tools with respect to the experimental phenomenology. The latter is recognized as one of the major gaps in going from a research stage to a production stage in thermonuclear fusion for energy production [43].

 

In this Letter, a solution to the unresolved issue recalled above is provided, based on a first principles model (nonlinear 3D viscoresistive MHD). The key ingredient is the use of helical BCs for the edge radial magnetic field $B_r$, consistent with a small helical modulation of the plasma magnetic boundary. Helical BCs with $m = 1$ poloidal and $n = -7$ toroidal periodicity are used, corresponding to the standard dominant mode in RFX-mod, the reference device in this Letter. The helical $B_r$ perturbation required for systematic QSH stimulation is comparable with the small (with respect to the edge mean field) dominant $B_r$ perturbation measured at the RFX-mod plasma boundary. Qualitative agreement between MHD simulation and experiment is obtained regarding topological properties of helical states, and quantitative agreement is approached concerning the level of the dominant and secondary modes.

Numerical simulations are performed with the 3D MHD code SPECYL [32,37], which was the subject of a recent thorough nonlinear verification study [44]. The code solves the viscoresistive MHD model in cylindrical geometry in the zero-$\beta$, constant-density approximation, whose equations in dimensionless units are

$$\frac{\partial \mathbf{B}}{\partial t} = \nabla \times (\mathbf{v} \times \mathbf{B} - \eta \mathbf{J}), \tag{1}$$

$$\frac{\partial \mathbf{v}}{\partial t} + (\mathbf{v} \cdot \nabla)\mathbf{v} = \mathbf{J} \times \mathbf{B} + \nu \nabla^2 \mathbf{v}, \tag{2}$$

together with $\nabla \cdot \mathbf{B} = 0$ and $\mathbf{J} = \nabla \times \mathbf{B}$. In these units, the radial coordinate $r$ is normalized to the minor radius $a$ of the rectified torus (with poloidal and toroidal-like coordinates $\theta$ and $\phi$ and major radius $R$ such that the aspect ratio is $R/a = 4$ as in RFX-mod), time $t$ and velocity $\mathbf{v}$ are normalized to the on-axis Alfvén time $\tau_A$ and velocity $v_A$, and the magnetic field $\mathbf{B}$ is normalized to the initial value of the toroidal magnetic field $B_0$ on axis. The on-axis resistivity and viscosity are the inverse Lundquist number $\eta_0 = \tau_A/\tau_R \equiv S^{-1}$ and the inverse viscous Lundquist number $\nu_0 = \tau_A/\tau_V \equiv M^{-1}$, respectively ($\tau_R$ and $\tau_V$ being the resistive and viscous time scales). $\nu$ is assumed to be uniform, while an increasing radial profile is assigned for $\eta$, of the form $\eta(r) = \eta_0[1 + 19(r/a)^{10}]$. A wide spectrum of 225 modes with $0 \le m \le 4$ is used. This spectrum was employed and validated in previous simulation studies [32,37,44]. As for the $m = 0$ and $m = 1$ modes, which are the most important in the nonlinear RFP dynamics, we use $-25 \le n \le 1$ and $-55 \le n \le 10$, respectively. The BCs at $r = a$ are such that the volume-averaged toroidal magnetic field $\langle B_\phi \rangle$ (proportional to the toroidal magnetic flux) and the externally imposed toroidal electric field $E_0$ are constant in time. The edge radial magnetic field may either be $B_r(a) = 0$ or helically modulated. The last condition was recently shown to favor Ohmic RFP equilibrium solutions [45]. A first assessment resulting from a systematic numerical study of the effect of helical BCs in nonlinear MHD simulations of the RFP is reported in Refs. [46,47].

We first consider a reference simulation with ideal BCs. The on-axis Lundquist and viscous Lundquist numbers are set to $S = 10^6$ and $M = 10^4$, respectively. This corresponds to Hartmann and Prandtl numbers $H \equiv (SM)^{1/2} = 10^5$ and $P \equiv S/M = 100$, respectively. The initial condition is a nonreversed axis-symmetric Ohmic equilibrium with pinch parameter $\Theta = B_\theta(a)/\langle B_\phi \rangle \simeq 1.6$ and reversal parameter $F = B_\phi(a)/\langle B_\phi \rangle \simeq 0.15$, where $\langle \cdot \rangle$ represents a volume average. The temporal evolution of the reversal parameter $F$ and the normalized edge $B_\phi$ amplitudes of the most active $m = 1$ modes is shown in Figs. 1(a) and 1(b). The resulting sawtoothing dynamics closely reproduces what was already reported in past viscoresistive MHD studies with similar ideal BCs [32–37]. After a strong initial reconnection event leading to the reversal of the $F$ parameter (i.e., to the formation of the RFP configuration), the system undergoes quasiperiodic cycles with reconnection events, associated with formation of current sheets and a strong nonlinear dynamo activity that flattens the current density mean profile and deepens the reversal. This is followed by relatively longer phases with reduced MHD activity, in which the current density peaks on a resistive time scale and the reversal becomes shallower. In this simulation, the MH regime is typically observed in between reconnection events, while QSH phases occasionally occur, although

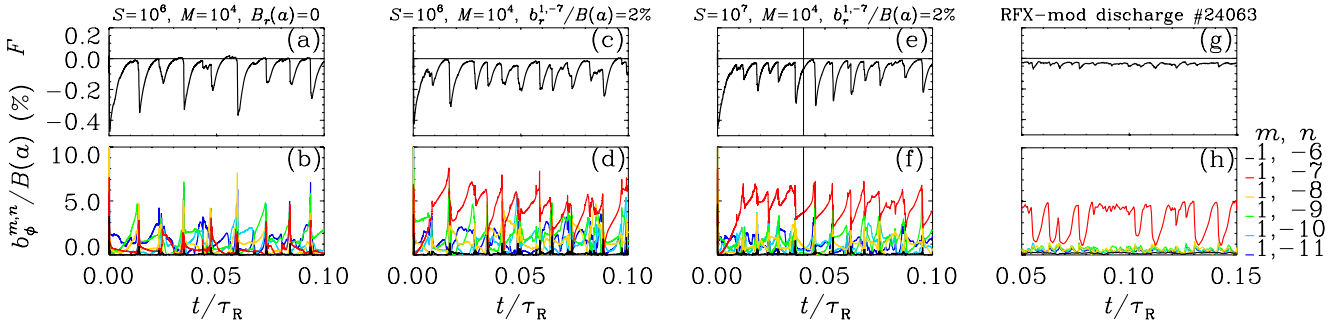


FIG. 1 (color online). MHD simulations with (a)–(b) $S = 10^6$, $M = 10^4$, and ideal BCs $B_r(a) = 0$; (c)–(d) $S = 10^6$, $M = 10^4$, and helical BCs $b_r^{1,-7}/B(a) = 2\%$; (e)–(f) $S = 10^7$, $M = 10^4$, and helical BCs $b_r^{1,-7}/B(a) = 2\%$. (g)–(h) RFX-mod discharge #24063 with flat-top averaged plasma parameters $I_P \simeq 1.5$ MA, $n_e \simeq 2.8 \times 10^{19}$ m$^{-3}$, $T_e \simeq 750$ eV, and $S \simeq 1.5 \times 10^7$ (cf. Ref. [14]). The temporal evolution of (first row) the reversal parameter $F$ and (second row) the edge $B_\phi$ amplitudes of the main $m = 1$ harmonics, normalized to the mean edge magnetic field, is reported.

without any specific dominant mode and with a rather small amplitude separation with respect to secondary modes.

A qualitative change occurs with the inclusion of helical BCs. We consider a first simulation with the addition of a helical perturbation of the edge radial magnetic field. This perturbation is chosen with $m = 1, n = -7$ periodicity and a constant in time amplitude around 2% of the mean edge field. Such BCs provide a schematic representation of the plasma magnetic boundary during high current discharges in RFX-mod. In fact, the time-averaged, normalized edge $B_r$ amplitude of the dominant mode can take values up to 1.5% for the standard RFX-mod operation, where the magnetic feedback system minimizes the edge $B_r$ amplitude of each harmonic [48]. Similarly, values up to 3% of this quantity have been reached in recent experimental operation employing external helical shaping [49]. The temporal evolution of the simulation with helical BCs is shown in Figs. 1(c) and 1(d). It can be clearly seen that QSH phases with 1, −7 dominant mode regularly occur in between reconnection events, while MH conditions seldom intervene. Thus, the observed numerical QSH dynamics presents the peculiar experimental features missing in previous modeling. For comparison, a typical RFX-mod discharge with standard feedback control at high current is shown in Figs. 1(g) and 1(h). The finite helical $B_r$ perturbation also affects the periodic sawtoothing activity of the reversal parameter $F$, which on average becomes more frequent and less intense. This trend is confirmed for increasing helical perturbation amplitudes [47]. The quantitative agreement between experiment and MHD simulations also improves, concerning, in particular, the amplitude of the dominant mode. In fact, the normalized edge $B_\phi$ amplitude of the dominant mode is mostly dependent on the level of the helical BC [47], and takes realistic values for realistic edge $B_r$ amplitudes. The main quantitative differences with respect to experimental findings are the wider range of numerical $F$ oscillations and the larger level of secondary modes. The average total amplitude of secondary modes (computed as in Ref. [14]) is in fact 3.7% in this MHD simulation, instead of being around or even below 1% as in the experiment. This difference is mainly due to the use of unrealistic dissipation parameters. In particular, Lundquist numbers of the order of $S = 10^7$ have been obtained in RFX-mod [14]. The effect of increasing the Lundquist number is illustrated in Figs. 1(e) and 1(f), where a simulation with the same parameters as before but $S = 10^7$ (corresponding to $H \simeq 3 \times 10^5$ and $P = 10^3$) is reported. This simulation case is qualitatively similar to the previous one. However, the average total amplitude of secondary modes decreases to 2.9%. This makes the repetition of QSH phases in between reconnection events particularly clear and systematic. In fact, QSH phases turn out to occur always in between reconnection events, with a close to realistic amplitude separation with respect to secondary modes.

The dependence of the average total secondary modes amplitude on dissipation parameters is reported in Fig. 2, showing data from a set of MHD simulations with the same 2% magnetic perturbation amplitude and varying $S$ and $M$ numbers. First of all, the level of secondary modes decreases with both $S$ and $M$. In addition, as expected since the Hartmann number is the main parameter ruling the viscoresistive MHD dynamics [31,32], the points nearly collapse on the same line when plotted as a function of $H$. In fact, the total amplitude of secondary modes scales like $b_\phi^{1,\mathrm{secd}}/B(a) \sim H^{-0.22}$. When expressed as a function of the parameter couple ($S$, $M$), this scaling becomes $b_\phi^{1,\mathrm{secd}}/B(a) \sim S^{-0.11}M^{-0.11}$. On the other hand, when considering the couple ($S$, $P$), secondary modes scale like $S^{-0.22}P^{0.11}$. These scalings are quite close to those obtained for magnetic fluctuations in past MHD studies with standard ideal wall conditions, namely $S^{-0.22}$ at fixed $P = 1$ [37,50] and $S^{-0.14}$ at (basically) fixed $M$ [51]. This agreement is consistent with the observed weak dependence of secondary modes on the helical magnetic perturbation amplitude [47]. A quantitative comparison with the experimental trend of secondary modes with $S^{-0.35}$ [14] is complicated by the difficulty in estimating the experimental viscosity. However, since MHD simulations show a rather weak scaling of secondary modes with $S$ at fixed $M$, and the scaling at fixed $P$ is closer to the experimental trend, we infer a hidden viscosity effect in the experimental dependence of secondary modes on $S$. The indication of a nearly fixed $P$ is also compatible with the classical theoretical estimate of the perpendicular Prandtl number [50], suggesting a rather constant $P_\perp$ vs plasma current in the RFP (on the other hand, a strong increase of the parallel Prandtl number $P_\parallel$ is predicted). Nevertheless, it must be stressed that a direct quantitative matching with the experiment is beyond the scope of this Letter. In fact, the level of MHD modes is known to depend on the chosen resistivity profile, which is not found self-consistently within viscoresistive MHD [52]. Moreover, finite-$\beta$ and thermal transport effects [41,51] as well as two-fluid effects [42] are likely to introduce important quantitative differences with respect to our simple model. In particular, a reduction by a factor of two in the amplitude of MHD modes is expected due to

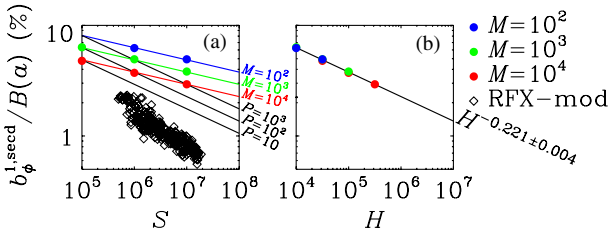


FIG. 2 (color online). Average total amplitude of secondary modes in MHD simulations with helical BCs $b_r^{1,-7}/B(a) = 2\%$ and varying $S$ and $M$ parameters, plotted with full circles vs (a) $S$ and (b) $H$. The line in panel (b) is the fit of the amplitude of secondary modes vs $H$, while the colored and black lines in panel (a) show the same fit expressed as a function of $S$ at fixed $M$ and $P$, respectively. The total amplitude of secondary modes in RFX-mod QSH plasmas is plotted in panel (a) with open diamonds (adapted from Ref. [14]).

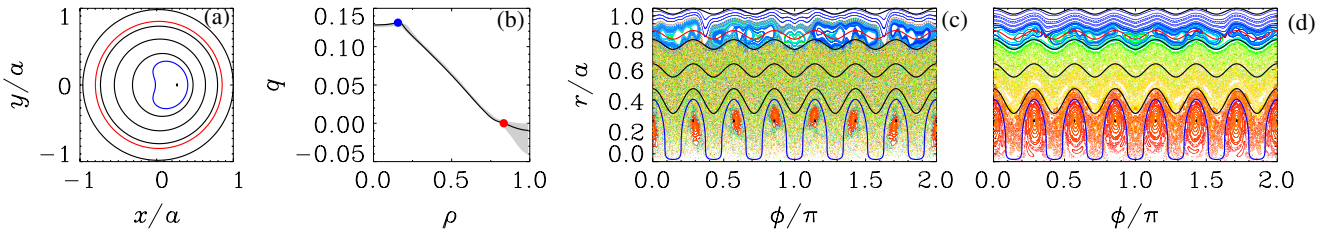


FIG. 3 (color online). Topological analysis of the magnetic configuration at the marked simulation time in Figs. 1(e) and 1(f) showing (a) contour levels of the normalized helical flux function $\rho$ such that $\nabla\rho \cdot \mathbf{B}_h = 0$, where $\mathbf{B}_h$ is the helical symmetric part of $\mathbf{B}$ with geometric helicity $n/m = -7$; (b) helical safety factor $q(\rho) = (d\Phi)/(d\psi)$, where $\Phi(\rho)$ and $\psi(\rho)$ are the toroidal and poloidal flux of $\mathbf{B}_h$ across the helical flux surface $\rho$, respectively; Poincaré plots on $r$-$\phi$ cross-section with (c) secondary modes with actual amplitudes and (d) secondary modes with amplitudes divided by 4. Black contour levels in panel (a) correspond to $\rho = 0, 0.25, 0.5, 0.75, 1$. Blue and red levels refer to $(dq)/(d\rho) = 0$ and $q = 0$, respectively. The gray shaded area in panel (b) represents the time variation of $q$ during a sawtooth cycle. Contour levels of $\rho$ are displayed on top of the Poincaré plots with the same color code as in panel (a).

warm-ion effects [42], which would bring the level of secondary modes closer to the experimental value.

Coming back to the MHD simulation reported in Fig. 1(e) and 1(f), the qualitative agreement with experimental findings is also noticeable when looking at the topological properties of the magnetic configuration. This is shown in Fig. 3 for a typical QSH phase in between reconnection events. Concerning the helical flux surfaces, a SHAx state with a helical core enclosed by an almost axis-symmetric edge is observed, as in the experiment [10]. The helical $q$ profile, computed as described in [53], is also similar to the experimental estimates for SHAx states, being characterized by a reversal of the magnetic shear in the core region [54–57]. The topology of the total magnetic field is qualitatively similar with experimental estimates as well. The latter are characterized by conserved structures in the helical core enclosed by a chaotic region at intermediate radius [14,24,58] and by the typical chain of $m = 0$ islands at the edge [59–62]. Poincaré plots on a toroidal cross section are reported in Figs. 3(c) and 3(d), as computed with the field-line tracing code NEMATO [53,63,64] by using the full spectrum of modes from the MHD simulation. If the actual secondary mode amplitudes are taken into account, conserved helical structures in the core are rather narrow and the core region turns out to be topologically connected with the plasma edge. However, if the amplitude of secondary modes is divided by a factor of four in the NEMATO computation in order to approximately match the average experimental amplitude, the conserved core region broadens, a transport barrier [65] appears at $\rho = 0.25$, and the $q = 0$ surface provides a topological separation between the plasma core and the wall. The inclusion of toroidal coupling is essential to recover the experimentally observed $m = 0$, $n = 7$ island chain at the reversal surface [60,62], as confirmed by preliminary simulations with the MHD code PIXIE3D [66] in toroidal geometry [67,68]. Overall, the topological analysis performed on the simulation set presented here, which aims at a realistic representation of RFX-mod, strengthens the trend observed in the general assessment study of Ref. [47]. Such a result suggests that conserved core structures should be found in SHAx states with realistic mode amplitudes even when considering the full spectrum of MHD modes, which was recently questioned based on RFX-mod experimental reconstructions taking into account up to $m = 2$ modes [69].

In conclusion, a major step towards qualitative and quantitative agreement of viscoresistive MHD simulations of the RFP with respect to experimental findings has been reported in this Letter. This Letter teaches us that, similar to what was observed for the velocity BCs in the fluid dynamics context [70], the BCs for the magnetic field have a strong impact in the MHD modeling of RFP plasmas. With suitable magnetic BCs, the viscoresistive MHD model is indeed able to capture the dominant physics of experimental QSH plasmas. This helps us to understand how helical self-organization in the RFP works, and how it can be exploited to improve the confinement properties of this configuration. Why the $n = -7$ mode is the dominant one in RFX-mod plasmas is still not understood. However, we believe that the solution to this and other related open questions will come by following the avenue of research opened in this Letter, i.e., by the use of refined plasma models together with a realistic description of the magnetic boundary.

This work was supported by the Euratom Communities under the contract of Association between EURATOM/ENEA. The views and opinions expressed herein do not necessarily reflect those of the European Commission.

*daniele.bonfiglio@igi.cnr.it

[1] D. Biskamp, *Nonlinear Magnetohydrodynamics* (Cambridge University Press, Cambridge, England, 1993).
[2] S. Ortolani and D. D. Schnack, *Magnetohydrodynamics of Plasma Relaxation* (World Scientific, Singapore, 1993).
[3] J. Wesson, *Tokamaks* (Oxford University Press, New York, 2004), 3rd ed.
[4] D. J. Den Hartog, J. T. Chapman, D. Craig, G. Fiksel, P. W. Fontana, S. C. Prager, and J. S. Sarff, Phys. Plasmas **6**, 1813 (1999).
[5] D. Bonfiglio, S. Cappello, and D. F. Escande, Phys. Rev. Lett. **94**, 145001 (2005).
[6] S. Cappello, D. Bonfiglio, and D. F. Escande, Phys. Plasmas **13**, 056102 (2006).
[7] K. A. Werley, Nucl. Fusion **31**, 567 (1991).

[8] D. F. Escande *et al.*, Phys. Rev. Lett. **85**, 1662 (2000).
[9] P. Martin *et al.*, Nucl. Fusion **43**, 1855 (2003).
[10] R. Lorenzini *et al.*, Nat. Phys. **5**, 570 (2009).
[11] J. S. Sarff *et al.*, in *Proceedings of the 24th IAEA Fusion Energy Conference, San Diego, USA* (2012) http://www-naweb.iaea.org/napc/physics/FEC/FEC2012/papers/452_OV52Ra.pdf.
[12] P. Sonato *et al.*, Fusion Eng. Des. **66–68**, 161 (2003).
[13] R. N. Dexter, D. W. Kerst, T. W. Lovell, S. C. Prager, and J. C. Sprott, Fusion Technol. **19**, 131 (1991).
[14] P. Piovesan *et al.*, Nucl. Fusion **49**, 085036 (2009).
[15] B. E. Chapman *et al.*, in *Proceedings of the 24th IAEA Fusion Energy Conference, San Diego, USA* (2012) http://www-naweb.iaea.org/napc/physics/FEC/FEC2012/papers/622_EXP601.pdf.
[16] W. F. Bergerson *et al.*, Phys. Rev. Lett. **107**, 255001 (2011).
[17] L. Delgado-Aparicio *et al.*, Phys. Rev. Lett. **110**, 065006 (2013).
[18] W. A. Cooper, J. P. Graves, and O. Sauter, Plasma Phys. Controlled Fusion **53**, 024002 (2011).
[19] L. Spitzer, Phys. Fluids **1**, 253 (1958).
[20] A. H. Boozer, Phys. Plasmas **5**, 1647 (1998).
[21] P. Helander *et al.*, Plasma Phys. Controlled Fusion **54**, 124009 (2012).
[22] D. L. Meier, S. Koide, and Y. Uchida, Science **291**, 84 (2001).
[23] S. E. Gibson, Y. Fan, T. Török, and B. Kliem, Space Sci. Rev. **124**, 131 (2006).
[24] R. Lorenzini, D. Terranova, A. Alfier, P. Innocente, E. Martines, R. Pasqualotto, and P. Zanca, Phys. Rev. Lett. **101**, 025005 (2008).
[25] S. Choi, D. Craig, F. Ebrahimi, and S. C. Prager, Phys. Rev. Lett. **96**, 145004 (2006).
[26] M. Zuin, N. Vianello, M. Spolaore, V. Antoni, T. Bolzonella, R. Cavazzana, E. Martines, G. Serianni, and D. Terranova, Plasma Phys. Controlled Fusion **51**, 035012 (2009).
[27] N. A. Crocker, G. Fiksel, S. C. Prager, and J. S. Sarff, Phys. Rev. Lett. **90**, 035003 (2003).
[28] S. Cappello and R. Paccagnella, in *Proceedings of the Workshop on Theory of Fusion Plasmas*, edited by E. Sindoni (Compositori, Bologna, 1990), p. 595.
[29] S. Cappello and R. Paccagnella, Phys. Fluids B **4**, 611 (1992).
[30] J. M. Finn, R. Nebel, and C. Bathke, Phys. Fluids B **4**, 1262 (1992).
[31] S. Cappello and D. F. Escande, Phys. Rev. Lett. **85**, 3838 (2000).
[32] S. Cappello, Plasma Phys. Controlled Fusion **46**, B313 (2004).
[33] A. Y. Aydemir and D. C. Barnes, Phys. Rev. Lett. **52**, 930 (1984).
[34] D. D. Schnack, E. J. Caramana, and R. A. Nebel, Phys. Fluids **28**, 321 (1985).
[35] K. Kusano and T. Sato, Nucl. Fusion **30**, 2075 (1990).
[36] Y. L. Ho and G. G. Craddock, Phys. Fluids B **3**, 721 (1991).
[37] S. Cappello and D. Biskamp, Nucl. Fusion **36**, 571 (1996).
[38] J. A. Reusch, J. K. Anderson, D. J. Den Hartog, F. Ebrahimi, D. D. Schnack, H. D. Stephens, and C. B. Forest, Phys. Rev. Lett. **107**, 155002 (2011).
[39] D. J. Den Hartog *et al.*, in *Proceedings of the 24th IAEA Fusion Energy Conference, San Diego, USA* (2012) http://www-naweb.iaea.org/napc/physics/FEC/FEC2012/papers/209_EXP317.pdf.
[40] P. Paccagnella, D. Terranova, and P. Zanca, Nucl. Fusion **47**, 990 (2007).
[41] M. Onofri, F. Malara, and P. Veltri, Phys. Plasmas **18**, 052502 (2011).
[42] J. R. King, C. R. Sovinec, and V. V. Mirnov, Phys. Plasmas **19**, 055905 (2012).
[43] M. Greenwald, Phys. Plasmas **17**, 058101 (2010).
[44] D. Bonfiglio, L. Chacón, and S. Cappello, Phys. Plasmas **17**, 082501 (2010).
[45] D. Bonfiglio, D. F. Escande, P. Zanca, and S. Cappello, Nucl. Fusion **51**, 063016 (2011).
[46] M. Veranda, Ph.D. thesis, Università degli Studi di Padova, 2013.
[47] M. Veranda, D. Bonfiglio, S. Cappello, L. Chacón, and D. F. Escande, Plasma Phys. Controlled Fusion **55**, 074015 (2013).
[48] P. Zanca, L. Marrelli, G. Manduchi, and G. Marchiori, Nucl. Fusion **47**, 1425 (2007).
[49] P. Piovesan *et al.*, Plasma Phys. Controlled Fusion **53**, 084005 (2011).
[50] D. Terranova, T. Bolzonella, S. Cappello, P. Innocente, L. Marrelli, and R. Pasqualotto, Plasma Phys. Controlled Fusion **42**, 843 (2000).
[51] J. Scheffel and D. D. Schnack, Nucl. Fusion **40**, 1885 (2000).
[52] H.-E. Sätherblom, S. Mazur, and P. Nordlund, Plasma Phys. Controlled Fusion **38**, 2205 (1996).
[53] D. Bonfiglio, M. Veranda, S. Cappello, L. Chacón, and G. Spizzo, J. Phys. Conf. Ser. **260**, 012003 (2010).
[54] M. E. Puiatti *et al.*, Plasma Phys. Controlled Fusion **51**, 124031 (2009).
[55] D. Terranova *et al.*, Plasma Phys. Controlled Fusion **52**, 124023 (2010).
[56] M. Gobbin, D. Bonfiglio, D. F. Escande, A. Fassina, L. Marrelli, A. Alfier, E. Martines, B. Momo, and D. Terranova, Phys. Rev. Lett. **106**, 025001 (2011).
[57] M. Gobbin *et al.*, Phys. Plasmas **18**, 062505 (2011).
[58] I. Predebon, L. Marrelli, R. B. White, and P. Martin, Phys. Rev. Lett. **93**, 145001 (2004).
[59] G. Spizzo, S. Cappello, A. Cravotta, D. Escande, I. Predebon, L. Marrelli, P. Martin, and R. B. White, Phys. Rev. Lett. **96**, 025001 (2006).
[60] G. Spizzo *et al.*, Plasma Phys. Controlled Fusion **52**, 095011 (2010).
[61] E. Martines, R. Lorenzini, B. Momo, S. Munaretto, P. Innocente, and M. Spolaore, Nucl. Fusion **50**, 035014 (2010).
[62] P. Scarin *et al.*, Nucl. Fusion **51**, 073002 (2011).
[63] J. M. Finn and L. Chacón, Phys. Plasmas **12**, 054503 (2005).
[64] G. Ciaccio, M. Veranda, D. Bonfiglio, S. Cappello, G. Spizzo, L. Chacón, and R. B. White, Phys. Plasmas **20**, 062505 (2013).
[65] R. S. MacKay, J. D. Meiss, and I. C. Percival, Phys. Rev. Lett. **52**, 697 (1984).
[66] L. Chacón, Phys. Plasmas **15**, 056103 (2008).
[67] S. Cappello *et al.*, Nucl. Fusion **51**, 103012 (2011).
[68] S. Cappello *et al.*, in *Proceedings of the 24th IAEA Fusion Energy Conference, San Diego, USA* (2012) http://www-naweb.iaea.org/napc/physics/FEC/FEC2012/papers/199_THP216.pdf.
[69] L. Carraro *et al.*, in *Proceedings of the 24th IAEA Fusion Energy Conference, San Diego, USA* (2012) http://www-naweb.iaea.org/napc/physics/FEC/FEC2012/papers/105_EXP304.pdf.
[70] S. Li, D. Montgomery, and W. B. Jones, Theor. Comput. Fluid Dyn. **9**, 167 (1997).